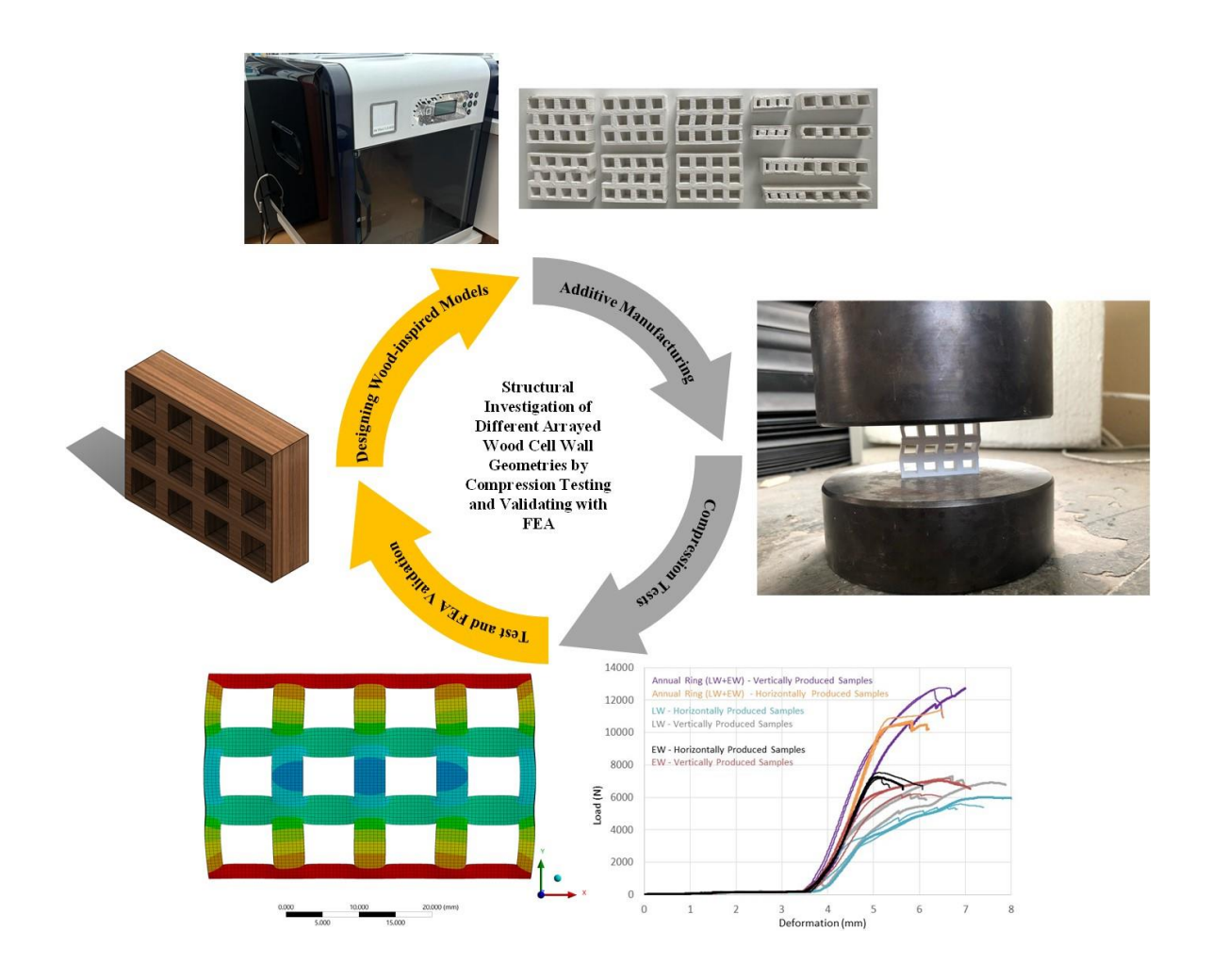
Structural Investigation of Wood-Inspired Cell Wall Geometries Using Additive Manufacturing: Compression Testing and Finite Element Analysis Validation

Murat Aydin, and Yasin Furkan Gorgulu

*Corresponding author: yasingorgulu@isparta.edu.tr

DOI: 10.15376/biores.19.4.7493-7512

GRAPHICAL ABSTRACT



Structural Investigation of Wood-Inspired Cell Wall Geometries Using Additive Manufacturing: Compression Testing and Finite Element Analysis Validation

Murat Aydin, and Yasin Furkan Gorgulu*

Mechanical properties of wood-inspired cell wall geometries were considered through compression testing and Finite Element Analysis (FEA) with ANSYS simulation. Six models, including earlywood, latewood, and various array configurations, were fabricated via 3D printing using acrylonitrile butadiene styrene (ABS) filament. Compression tests highlighted the annual ring model's robustness, exhibiting a maximum load of 12707 MPa, while the 4x3 matrix displayed the lowest strength at 4247 MPa. Shifting rows led to reduced strength, which was particularly evident in vertical prints. An analysis of variance revealed significant differences in mechanical properties. Discrepancies between experimental tests and FEA results ranged from -45.9% to 35.2%. Earlywood exhibited a maximum deformation of 2.6 mm, whereas latewood showed lower deformation, indicating geometry's influence on material behavior. Mesh quality remained consistent, ensuring dependable simulation outcomes. These findings underscore the pivotal role of geometry in compression resistance, laying the groundwork for future studies on wood densification mechanisms and the development of customized wood composites.

DOI: 10.15376/biores.19.4.7493-7512

Keywords: 3D printing; Compression testing; Densification; FEA; Material strength.

Contact information: Department of Machinery and Metal Technologies, Keciborlu Vocational School, Isparta University of Applied Sciences, Isparta, Turkiye;

INTRODUCTION

One of the most important criteria determining the strength properties of wood material is the microstructure of wood cells (Chen *et al.* 2020; Toumpanaki *et al.* 2021; Yan *et al.* 2022). A wood cell wall usually consists of several layers (a primary layer and three secondary sublayers), and the microfibrils in each of these zones are oriented in different directions and geometries. Wood cells are composed of cell walls and lumens (the interior hollow or water-filled core spaces) and resemble an octagonal structure similar to a honeycomb structure (Yan *et al.* 2022) for hardwoods while they resemble rows of parallelograms with rounded corners in the case of softwoods. Chemically, the wood cell wall is considered a small-scale composite material consisting of cellulose, hemicellulose, and lignin (Kollmann *et al.* 1975; Isoeai *et al.* 1989). Within that composite, lignin and hemicelluloses form the matrix components. The task of these matrix components is to stick together and to strengthen the structure.

^{*} Corresponding author: yasingorgulu@isparta.edu.tr

The essential axes (longitudinal-L, Radial-R, and Tangential-T) of wood define the anisotropy of wood. The secondary cell wall layer is mainly responsible for the anisotropic behavior. The cellular porous solid structure of wood is thought to be responsible for its mechanical characteristics, and when the wood cell is loaded perpendicular to the grain direction, the molecular arrangement of polymer components inside the S2 sublayer becomes crucial because this sublayer has the greatest thickness. In essence, the orientation-dependent mechanical characteristics of the wood cells and subsequently of the wood itself are determined by the anisotropy of the microfibrils in the S2 layer (Kollmann *et al.* 1975; Yan *et al.* 2022).

Recently, additive manufacturing (AM) has been a way of producing goods with a similar appearance to wood or wood-based materials with the help of filaments that include wood flours or such elements. Laminate object manufacturing is the earliest technique of AM that uses paper (Gibson et al. 2021); therefore, manufactured objects look much like wood appearance and behave similarly to wood (Gebhardt 2011). Furthermore, printed goods or elements may be assumed to be the substitution of traditional wooden parts or structures (Gibson et al. 2021). Fused deposition modeling is one of the most used techniques of the AM that uses polymer-based filaments. It is expressed that the FDM can easily be used to form wood fibers, and in general, mechanical behavior comparable to wood can be obtained (Buonamici et al. 2019). The FDM technique uses different filaments made of polylactic acid (PLA), acrylonitrile butadiene styrene (ABS), polyethylene terephthalate (PET), and thermoplastic polyurethane (TPU), which present different physical and mechanical behaviors. However, accumulation of the fluidified filament requires attention due to printing failures, such as warping, which is particularly seen for ABS (Chua et al. 2017). Furthermore, it should be noted that the accumulation direction and alignment of the models may cause anisotropic structure in 3D printing.

When literature was reviewed, furniture or joint-related issues (Mai *et al.* 2022; Nicolau *et al.* 2022; Yilmaz Aydın 2022; Saad 2024; Ueda 2024), mimicking the cell structure of wood (Correa *et al.* 2015; Markstedt *et al.* 2019; Aydin and Aydin 2022), mechanical evaluation (Aydin 2024; Öztürk *et al.* 2024), warping behavior (Kam *et al.* 2019), bonding (Tomec *et al.* 2022), utilization of wood-plastic composites (Tomec *et al.* 2021; Tomec and Kariž 2022), and wood flour (Ibrahim *et al.* 2014; Zhang *et al.* 2016; Montalvo Navarrete *et al.* 2017; Tao *et al.* 2017; Kariz *et al.* 2018; Das *et al.* 2021) were evaluated over additively manufactured parts or structures.

Mechanical characterization of wood can be done destructively and non-destructively. Furthermore, numerical methods are attracting more attention nowadays due to their predictable properties without wasting material and requiring advanced test tools. Finite element modeling and analysis is one of the commonly applied practices for the predicting the anisotropic mechanical behavior of wood (Eslami *et al.* 2021; Hong *et al.* 2011; Yılmaz Aydın and Aydın 2017).

Nature is the inspiration source for humankind, and the trees or woods are structures that reflect the unique patterns. Annual rings (AR) of a tree are one of the reflections and store lots of knowledge within them. Biomimetic the AR using the AM and figuring out the influence of some irregularities of the AR on the compression behavior and comparing with the numerical modeling and analysis are the main objectives of this study. The 3D modeling, additive manufacturing, static testing, and numerical analysis are the workflow phases of this study.

EXPERIMENTAL

Wood Cell Geometry Design and Arrays

SolidWorks software (Dassault Systèmes S. A., Vélizy-Villacoublay, France) was used for the 3D modeling of simplified wood-based structures. The wall thickness and lumen diameters of the cells (without rounded corners indeed the real softwood structures have) in the earlywood (EW) and latewood (LW) for the models are presented in Fig. 1.

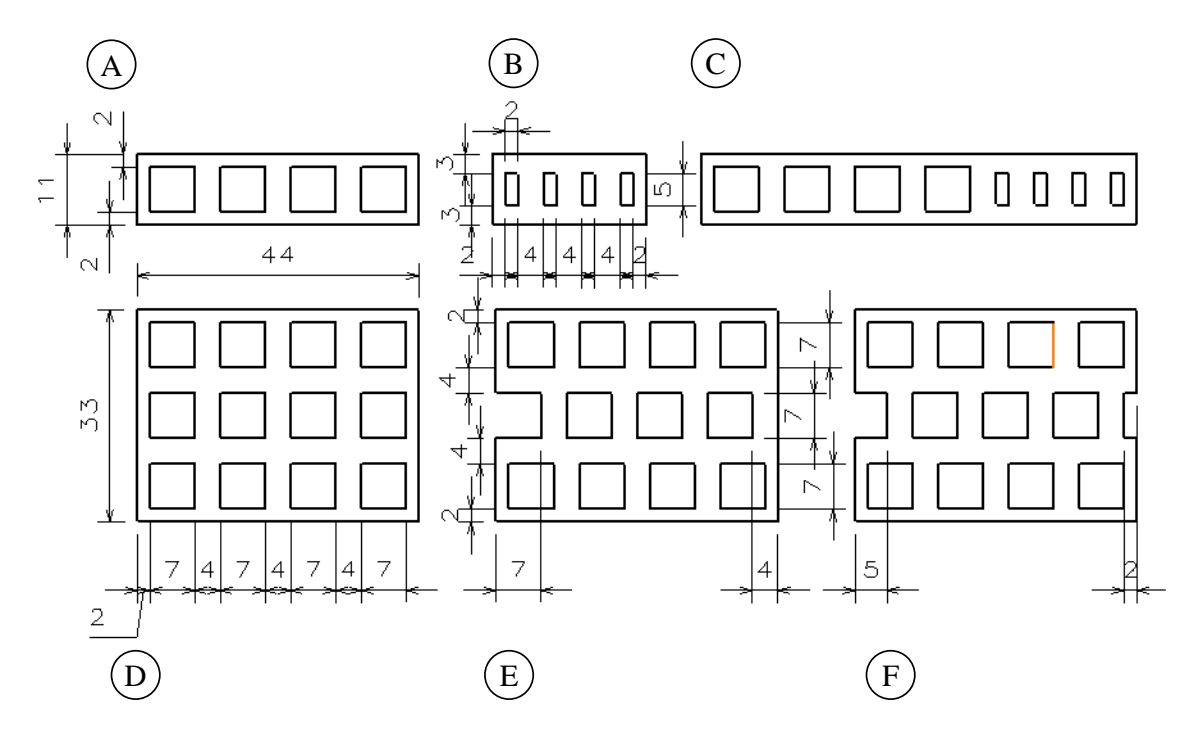


Fig. 1. Form and dimensions (mm) of the models

Six different 3D models (Fig. 1 A through F) of the wood-based structures were created to evaluate the differences between EW (Fig. 1A) and LW (Fig. 1B), and the influence of ring dislocation by 2 mm (Fig. 1E) and 4 mm (Fig. 1F) shifting the middle row of the control structure (Fig. 1D). The thickness of the models was 11 mm. As shown in Fig. 1, the cell wall thickness and lumen diameter of the models were 2 mm and 7 mm for EW models, respectively. For LW models, the cell wall thickness was 2 mm and the lumen dimension was 2×5 mm.

Additive Manufacturing

Solid 3D models were converted to Standard Triangle Language (STL) format for printing, and the models were sliced using XYZware software (XYZ Printing, New Kinpo Group, Taiwan).

Additive manufacture was carried out using a Da Vinci 1.0 AIO 3D printer (0.4 mm nozzle diameter, XYZ Printing, New Kinpo Group, Taiwan). All of the examples were printed at 100 µm resolution using the software's default, good printing parameters (30% infill density, rectilinear infill type, normal shell, 0.2 mm layer height, and slow speed). For layer accumulation, acrylonitrile butadiene styrene (ABS) filament with 1030 kg/m³ density and 1.075±0.05 mm diameter was employed. For the original XYZ ABS filament, the default temperatures for the nozzle and printing bed were around 214 °C and 90 °C,

respectively. To determine the effect of printing orientation, samples were printed vertical and horizontal alignments.

Compression Test

The ASTM D695 (2015) or ISO 604 (2002) standards were used to determine the rigid polymers' compression characteristics. However, the majority of studies evaluating 3D-printed samples did not perform experiments using such a standard.

Test specimens for compressive properties of rigid plastics are described in ASTMD695 (2015). The specimen sizes are $12.7 \times 12.7 \times 25.4$ mm³ and $10 \times 10 \times 4$ mm³ according to ASTM D695 (2015) and ISO 604 (2002), respectively. As shown in Fig. 1, the sizes of the samples were below the standard, particularly with ISO 604 (2002).

The compression properties of the wood-based constructions produced additively were ascertained by static compression testing without the need for a reference. The test was performed at 1.5 mm/min speed $(1.3 \pm 0.3 \text{ mm})$ is the standard testing speed according to ASTM D695 (2015)). A total of 36 samples for 6 different models were tested. Regarding ASTM D695 (2015), 5 and 10 samples should be tested for isotropic and anisotropic materials, respectively. Consequently, compression strength and strain values were determined. Furthermore, the obtained static results were compared with the results of numerical analysis (Finite Element Modeling and Analysis, FEM&A), which was performed using ANSYS R21 software.

Finite Element Analysis (FEA)

The compression of the wood cells was simulated using a commercial FEA program named ANSYS. Considering the microstructure of the wood and the nozzle structure of the 3D printer, larger scale models were used in simulation and experiments. Different cell structures and row numbers were considered in the created geometries. There were six models in total, the first three of which were single rows, the last three were three rows. The different cell wall models considered are given in Fig. 2. The heights of the wooden cell walls were kept constant; only their widths were changed. Model A had a width of 7 mm, and B had a width of 2 mm. C was designed as a combined version of them. Models D, E, and F were designed as three rows of A, but in E and F the middle row was offset by 2 and 4 mm, respectively. The material properties of the element used for modeling in the FEA are presented in Table 1.

Table 1. Properties of Plastic, ABS Used in the Analyses

Plastic, ABS				
Density	1030 kg/m³			
Young's Modulus	1628 MPa			
Poisson's Ratio	0.4089			
Bulk Modulus	2978.4 MPa			
Shear Modulus	577.76 MPa			
Secant Coefficient of Thermal Expansion	0.000184 1/°C			
Tensile Ultimate Strength	36.26 MPa			
Yield Strength	27.44 MPa			
Thermal Conductivity	0.0001997 W/mm.°C			
Specific Heat Constant Pressure	1.4×10 ³ J/kg.°C			

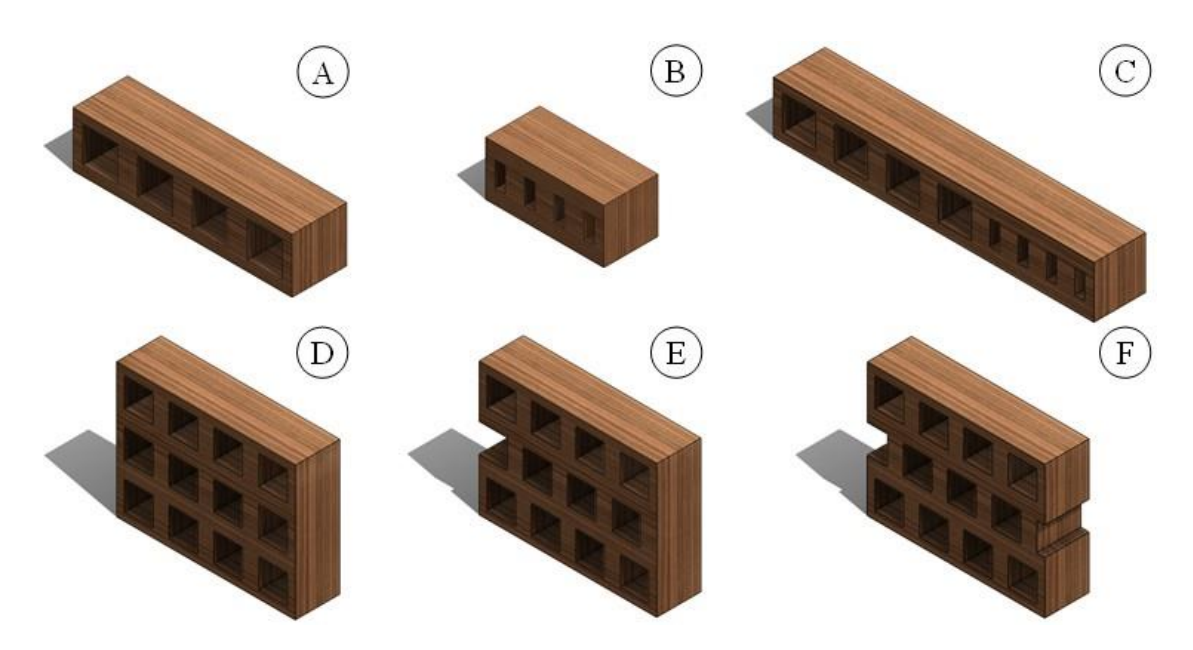


Fig. 2. A: Earlywood (EW), B: Latewood (LW), C: EW and LW combined, D: EW 4x3 Matrix, E: EW 4x3 Matrix, middle row shifted, F: EW 4x3 Matrix, middle row double-shifted

In the finite element analysis, the Ansys Static Structure module was used as the stress simulation computer program. The material subjected to compression was defined as elastoplastic material. Thus, when the force applied as a result of compression exceeds the elastic region of the material, permanent deformations can be observed by passing into the plastic region. Rigid compression plates were placed on the lower and upper sides of the test specimens to perform the compression action. The displacement of both compression plates was defined as 2.5 mm to compress the material, and a total displacement of 5 mm was defined. The sample material was defined as ABS (acrylonitrile butadiene styrene), which is also the material used in the experiments, and the compression process of 6 test samples formed after compression was carried out. The deformations, stress, and strain contours formed as a result of the FE (finite element) analysis were illustrated and compared to the experimental results.

Because there were six different geometries, six different simulations were done. Apart from the number of elements and nodes, their skewness and orthogonal qualities also varied. ANSYS recommends that the maximum skewness of a geometry be less than 0.95, and a value between 0 to 0.25 in the mesh quality spectrum is considered excellent. The minimum orthogonal quality, which is another criterion that determines the mesh quality, is required to be greater than 0.1. Orthogonal quality in the range of 0.95 to 1.0 is also given as excellent in this spectrum.

The fact that the geometries used were rectangular and the mesh preference was made in this direction has brought the skewness and orthogonal quality closer to the maximum quality. The mentioned values were also created for 6 geometries and are given in Table 2.

Specimen	Nodes	Elements	Maximum Skewness	Skewness Status	Minimum Orthogonal Quality	Orthogonal Quality Status
Α	140,733	32,146	5.48×10 ⁻⁷	Excellent	1.0	Excellent
В	102,589	23,794	4.68×10 ⁻⁷	Excellent	1.0	Excellent
С	239,145	55,122	4.70×10 ⁻⁷	Excellent	1.0	Excellent
D	368,261	82,834	3.28×10 ⁻⁴	Excellent	1.0	Excellent
E	367,354	82,834	7.76×10 ⁻⁴	Excellent	1.0	Excellent
F	367,354	82,834	4.50×10 ⁻⁴	Excellent	1.0	Excellent

Table 2. Mesh Metrics Table

To analyze the mechanical properties of cell walls during compression, stress, and strain are determined by the following equations (Cambaz *et al.* 2022; Yan *et al.* 2022),

$$\sigma_{nom} = \frac{F}{4} \tag{1}$$

$$\varepsilon_{nom} = \frac{d_{y}}{H} \tag{2}$$

where nominal stress (σ_{nom}) was calculated as the contact force between pressure plates (F) divided by the initial contact area between pressure plates (A). Nominal strain (ε_{nom}) is defined as the displacement (d_y) divided by the initial height of the specimen (H). Von-Mises stress, also known as effective stress, can be expressed as,

$$\sigma_{vm} = \sqrt{0.5[(\sigma_x - \sigma_y)^2 + (\sigma_y - \sigma_z)^2 + (\sigma_z - \sigma_x)^2] + 3(\tau_{xy}^2 + \tau_{yz}^2 + \tau_{zx}^2)}$$
 (3)

where σ_x , σ_y , and σ_z represent normal stresses, and τ_{xy} , τ_{yz} , τ_{zx} represent shear stresses.

RESULTS AND DISCUSSION

Compression Test Results

The statistics for the mechanical properties of the softwood inspired structures are presented in Table 3. A complete AR presented a higher load-carrying performance than EW and LW, while the worst was LW. The vertically printed AR was around 16.4% higher than that of horizontally printed. The same tendency was observed for LW. However, horizontally printed EW presented a 7.7% higher F_{max} . The F_{max} of LW was around 55.4% lower than that of AR. The F_{max} of horizontally printed LW was 22.6% lower than those of horizontally printed EW. However, there was a neglectable difference (0.2%) between EW and LW, which were vertically printed.

The load was applied perpendicular and parallel to the layers for vertically and horizontally printed samples, respectively. Due to the large hole size in EW models, vertical printing caused weak structure against the loading direction. This issue is assumed to have been a function of fiber direction and the size of the lumen, which is well-known in wood structures. The CS increases with the increase in tracheid wall thickness and decreases with the increase in tracheid diameter (Mańkowski and Laskowska 2021). As is well known, the CS order of the wood is Longitudinal > Radial > Tangential. Therefore, applying load through the fiber direction provides the highest values. For additively manufactured samples, this statement is false, because the alignment of the cells is not perpendicular to the applied load for horizontally printed samples. Therefore, these samples cannot be assumed as the L direction of the wood. However, vertically printed samples can be assumed as R-direction samples in terms of load application direction.

Contrary to F_{max} , LW presented the highest CS. As in F_{max} , vertical printing provided better performance. The EW presented the same opposite behavior in terms of printing orientation that is mentioned. The AR was around 43.4% and 45.6% lower than those of the LW and EW, respectively. The differences between EW and LW for CS ranged from 20.2% to 83.7%. Generally, it is expressed that the CS of EW is 50% of the CS of LW value for sapwood. Furthermore, the CS of LW in heartwood is around 2.5 times higher than the CS of EW (Mańkowski and Laskowska 2021). However, for EW models, CS values are closer to AR instead of being half. Furthermore, Chun-Won *et al.* (2001) reported 19.32 MPa, 79.7 MPa, and 457 MPa MOR values for EW, LW, and solid wood, respectively. The order and ratio between the MOR values do not match the results of this study. Except for CS, Büyüksari *et al.* (2017) reported that tensile strength values of LW for Scots pine is 3.2 times higher than EW.

According to Mańkowski and Laskowska (2021) there is no statistically significant difference between EW and LW for CS. However, as shown in Table 3, not only AR but also CS means of EW and LW models presented significant differences according to analysis of variance (ANOVA) results (P < 0.05).

Load and stress values at 5 mm elongation ranged from 3663 MPa (LW horizontally printed) to 9123 MPa (AR Horizontally printed), and 11.58 MPa (AR vertically printed) to 17.85 MPa (LW vertically printed), respectively. Wang *et al.* (2023) reported around 10, 8.5, and 14 MPa compressive stress for AR, EW, and LW of Douglas fir. The LW section of wood presented much higher compressive stress than EW and AR. The EW section presented slightly lower compressive stress than AR. However, when compared, the LW > EW > AR compressive stress order of this study did not agree with the reported data, particularly for AR *vs* EW. It should be taken into consideration that the compression of EW is easier because cell walls are thin and cell lumens are large; hence, the compressive stress of the AR is determined by the EW compressive stress (Wang *et al.* 2023).

Figure 3 shows that samples were buckled. Aydın (2023) observed buckling and shearing of AM small-sized samples. The same behavior was reported by Wang *et al.* (2023), who noted that rather than being flattened, buckling of the tracheid was observed in LW due to compression. The LW has thick and stiff cell walls that tend to bend in one direction.

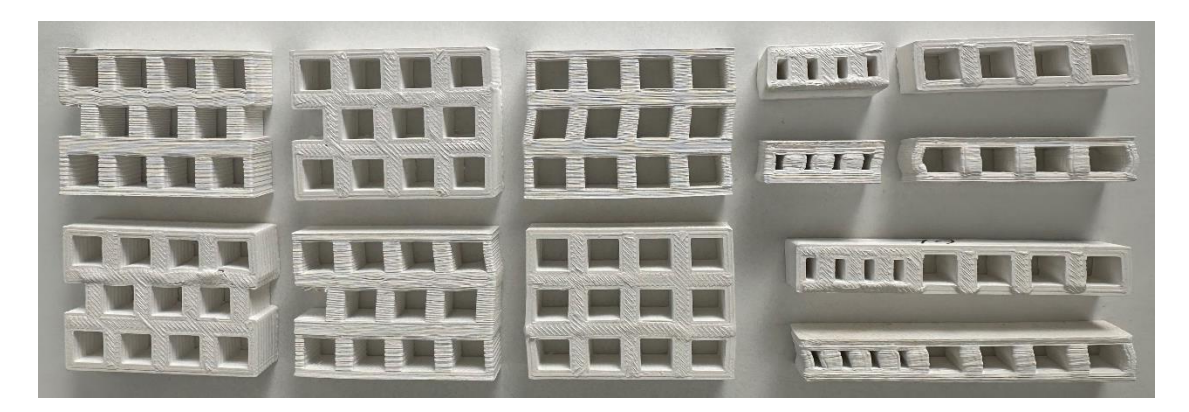


Fig. 3. Deformation of the samples

Generally, an increase in compressive ratio causes an increase in strain, and strain primarily concentrates on EW. A great amount of compression energy is absorbed by LW cells with a slight strain because of the highly stiff structure. The basic differences between

LW and EW are cell wall thickness, microfibril angle, and density, which make LW higher shear strength than LW (Li *et al.* 2021). Thus, the majority of the deformation is characterized by the more flexible EW (Wang *et al.* 2023).

In wood structure, as a naturally growing material, there is an inhomogeneous formation. Mechanical and processing properties of the wood are significantly influenced by the EW and LW share in a ring, as well as the transition of these distinctive sections, whether it is gradual or abrupt (Barbour 2004). As shown in the Fig. 1, there was no transition zone for AR and no inhomogeneity for the cell properties except for shifting. As a result, discrepancies in the coefficients of variations were small.

Sampl es	Printing Orienta- tion	F _{max} (N)*	CS* (MPa)	Load (N)* @ 5 mm Elongation	Stress (MPa)* @ 5 mm Elongation
AR	Vertical	12707 ^a [0.6]	16.99° [0.6]	8660° [11.83]	11.58° [11.83]
	Horizon- tal	10920 ^b [4]	14.60 ^d [4]	9123ª [2.97]	12.20° [2.97]
EW	Vertical	6800° [7.57]	14.05 ^d [7.57]	5777° [9.23]	11.98° [9.23]
	Horizon- tal	7323° [2.63]	15.13 ^{cd} [2.63]	7213 ^b [2.64]	14.90 ^b [2.64]
LW	Vertical	6813 ^c [8.04]	25.81 ^a [8.04]	4713 ^d [12.39]	17.85ª [12.39]
	Horizon- tal	5667 ^d [5.68]	21.46 ^b [5.68]	3663 ^e [6.83]	13.88 ^{bc} [6.83]

Table 3. Mechanical Properties EW, LW, and AR Structures

The statistics for the mechanical properties of the matrix structure are presented in Table 4. The uniform models (control) presented better performance than the shifted ones. However, either for vertical or horizontal printing, these values were significantly lower than the lowest values of EW, LW, and AR models. The ratio between the cross-section and height of the samples may have played a role in the decreased values. Because the matrix structure had a higher height, it may have caused a reduction in the resistance to load by deforming the layers' integrity. As shown in Fig. 1, the EW and matrix structure was the same in terms of cell and lumen properties. However, averages of the vertically and horizontally printed 4×3 matrix control samples presented 54.8% and 72.5% lower $F_{\rm max}$, respectively. The differences for CS were the same.

As is well known, there are disorders in the cell array of wood either in EW or LW, and it is assumed that this is one of the essential factors that influence the wood mechanical properties. As seen in Table 4, 2 and 4 mm shifting of the middle row of the matrix created disorder for EW configuration. Shifting caused 43.1% and 23.4% decreases in $F_{\rm max}$ for vertical and horizontal samples, respectively. The decreased percentages for CS were the same. Load at 5 mm deformation values were 29.5% and 23.1% decreased regarding vertical and horizontal alignment, respectively. The decrease in stress was the same. According to ANOVA (P < 0.05), differences between means for 4 × 3 matrix structures were statistically significant.

^{*} Duncan Homogeneity Groups, values in the brackets are the coefficient of variation

Sam- ples	Printing Orientation	F _{max} (N)*	CS (MPa)	Load (N) @ 5 mm Elongation	Stress (MPa) @ 5 mm Elongation
Con- trol	Vertical	4393 ^a [3.42]	9.08 ^a [3.42]	3333 ^b [13.68]	6.89 ^b [13.68]
	Horizontal	4247 ^a [7.09]	8.77 ^a [7.09]	4097ª [6.78]	8.46 ^a [6.78]
2 mm	Vertical	3093 ^b [9.84]	6.39 ^b [9.84]	2793 ^{bc} [8.8]	5.77 ^{bc} [8.8]
	Horizontal	3487 ^b [9.11]	7.20 ^b [9.11]	3303 ^b [8.52]	6.83 ^b [8.52]
4 mm	Vertical	2500° [6.44]	5.17 ^c [6.44]	2350° [1.28]	4.86° [1.28]
	Horizontal	3253 ^b [13.19]	6.72 ^b [13.19]	3150 ^b [15.74]	6.51 ^b [15.74]

Table 4. Mechanical Properties of the 4 × 3 Matrix Structure

Aydın (2023) observed plateau regions similar to those of this study (Figs. 4 and 5). It can be thought that the plateau region of the EW, LW, and AR must differ because the cell lumen size is not the same. Furthermore, LW and AR might present shorter plateau lengths. However, it is thought that printing parameters, such as infill density and type, are related to this strain occurring at low stress. Furthermore, not only do the mechanical characteristics of the filament dictate the mechanical attributes of the printed parts, but they also have an impact on the FDM processability, such as brittleness, which causes filament breaks and failure in printing (Chua *et al.* 2017). The infill density of the models was 30%. Therefore, it must be taken into consideration that there can be significant differences in the mechanical behavior between the additively manufactured models and solid ABS.

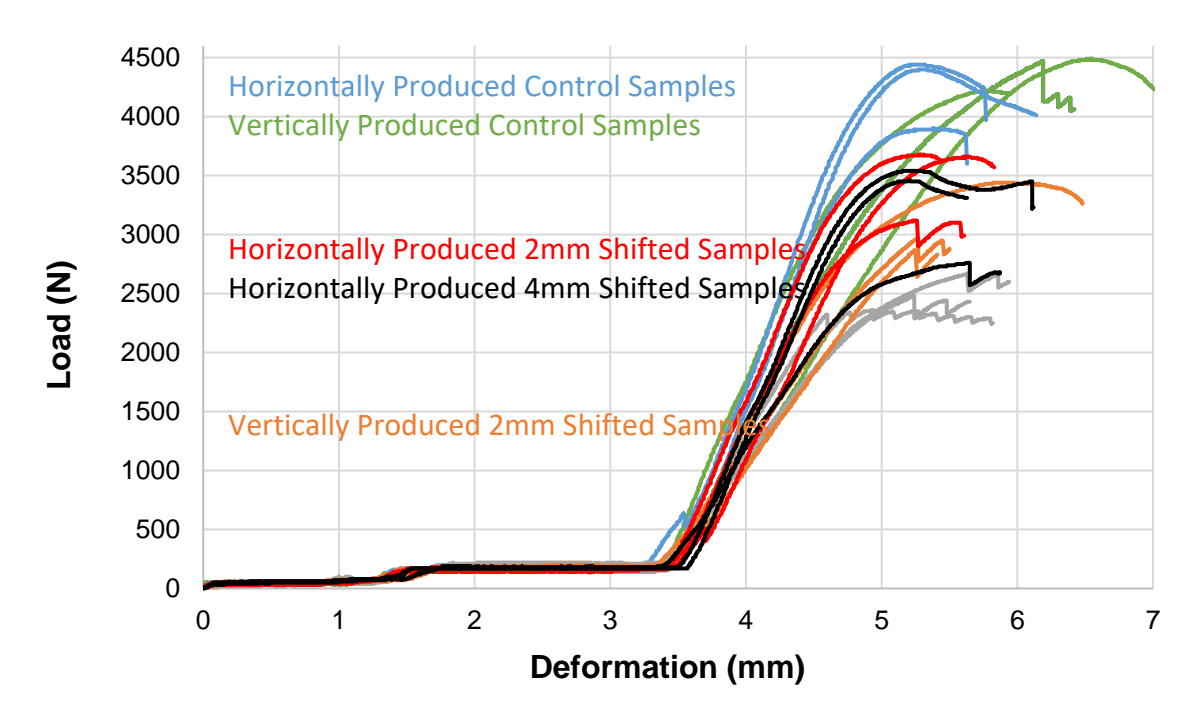


Fig. 4. Load deformation curves for the 4×3 ring structures

^{*} Duncan Homogeneity Groups, values in the brackets are the coefficient of variation

It is clear that from the load-deformation curves for all models, there were artifacts (toe regions) that occurred due to take-up of slack, and alignment or seating of the specimens. Therefore, to determine the correct zero point of strain, these artifacts should be compensated. However, this compensation must be applied in terms of linear (Hookean behavior) or nonlinear (no Hookean behavior) regions. As shown in Figs. 4 and 5, curves presented the Hookean regions. Therefore, the offset yield point is applicable with acceptable error.

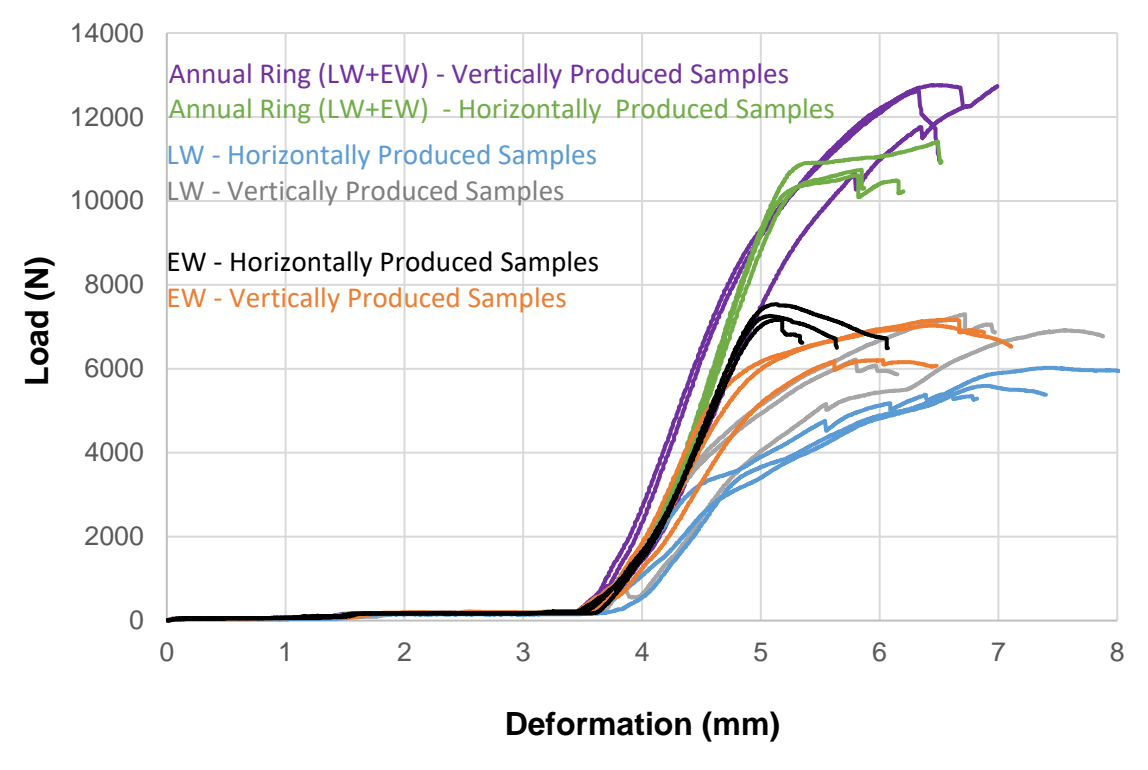


Fig. 5. Load deformation curves for EW, LW, and AR samples

In general, EW and LW present distinctive differences, and they ought to be assessed independently (van Buijtenen 2004). This study simulated this independent evaluation of EW and LW over additively manufactured wood-inspired cellular models. Models exhibited different load-deformation behaviors against the structure, reflecting the cellular formation of wood (earlywood, latewood, and annual rings). However, further investigation is needed to figure out the slope of the orientations, filament type, *etc*.

Finite Element Analysis Results

In the simulations, the displacement values were entered on the rigid compression plates, and thus these models were exposed to compression. Deformation, stress, and strain contours were reflected using the Ansys Static Structure module of six designed wood cell wall models. The aim of this work was to shed light on the mechanism of densification occurring in wood and find the necessary geometry to further strengthen it.

When the wood cell wall Type A is examined in Fig. 6, it is noteworthy that the highest deformation occurred on the surfaces where the pressure plates come into contact. It was seen that bending occurred on the outward-facing sides of the model, and compression-induced barreling occurred at other transition points, and their thickness increased.

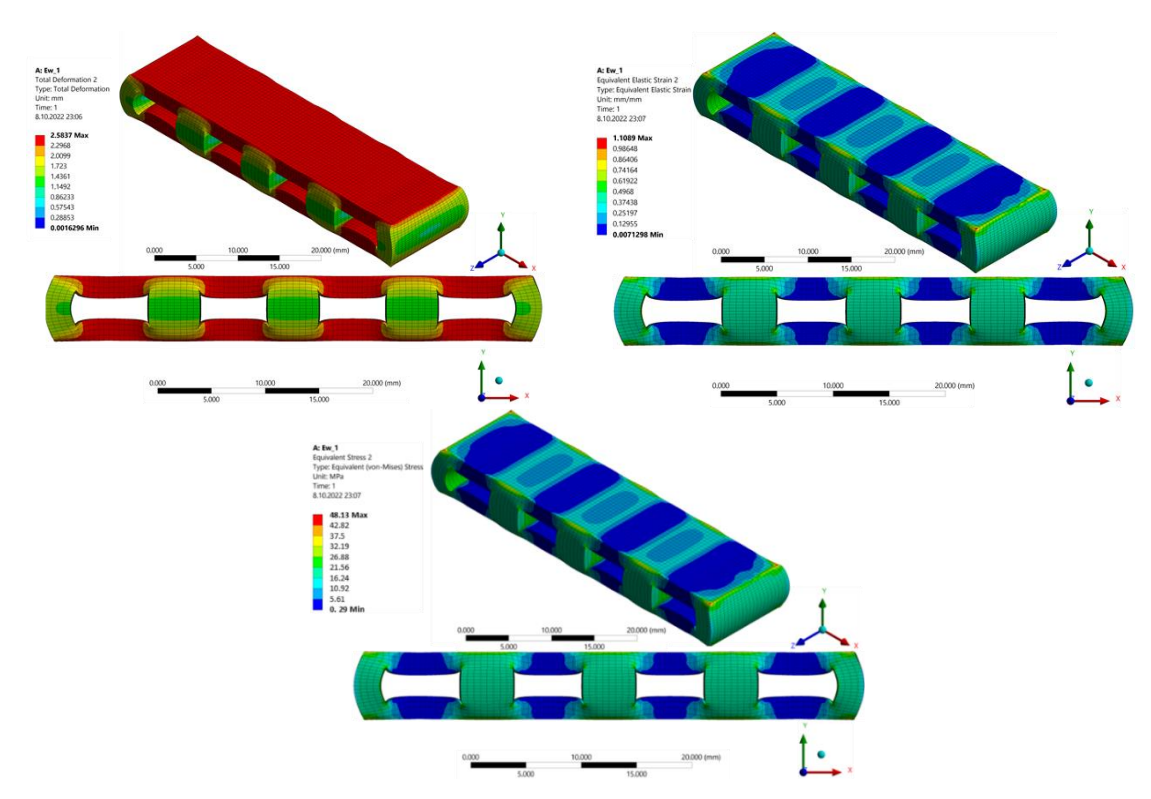


Fig. 6. Distributions of deformation, strain, and stress of wood cell wall Type A

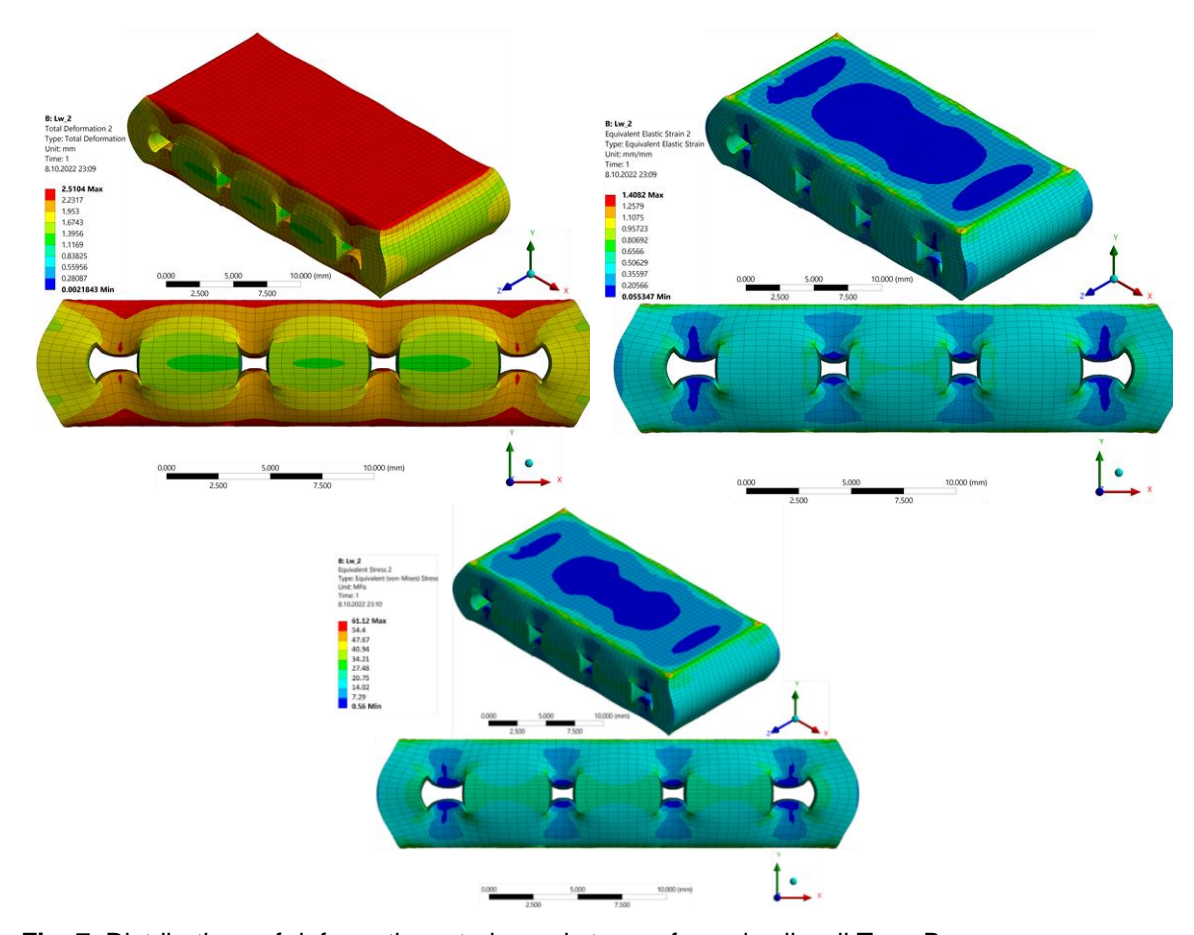


Fig. 7. Distributions of deformation, strain, and stress of wood cell wall Type B

The maximum deformation was approximately 2.6 mm at the contact points of the compression plates, and the minimum was 0.0016 mm on the inward-facing surfaces of the bridges. When the stress and strain contours were examined, a similar color distribution was observed. It was observed that the places where the stress was maximum were the sharp points and corners on the surfaces of the part where it contacted the pressure plates. In general, the areas where stress occurred were the places where the cell walls were linked to each other. It was seen that stresses and strains approached zero in the blank parts.

In the Type B sample, a high amount of barreling was observed. It seems that this barreling caused the holes in the test material to be almost closed. Wood cell Type B gave much lower deformation, stress, and strain compared to Type A. It can be seen that the maximum stress occurred on the facing surfaces of the hollow parts of the wood cell (see Fig. 7.).

Type C wood cell wall was formed by adding Type A and B to each other in series. Although it was composed of a combination of these two types, it showed higher strength properties even when evaluated individually. It was also observed that the symmetry of the stress and strain contours at the junction of the two wood cells was disturbed.

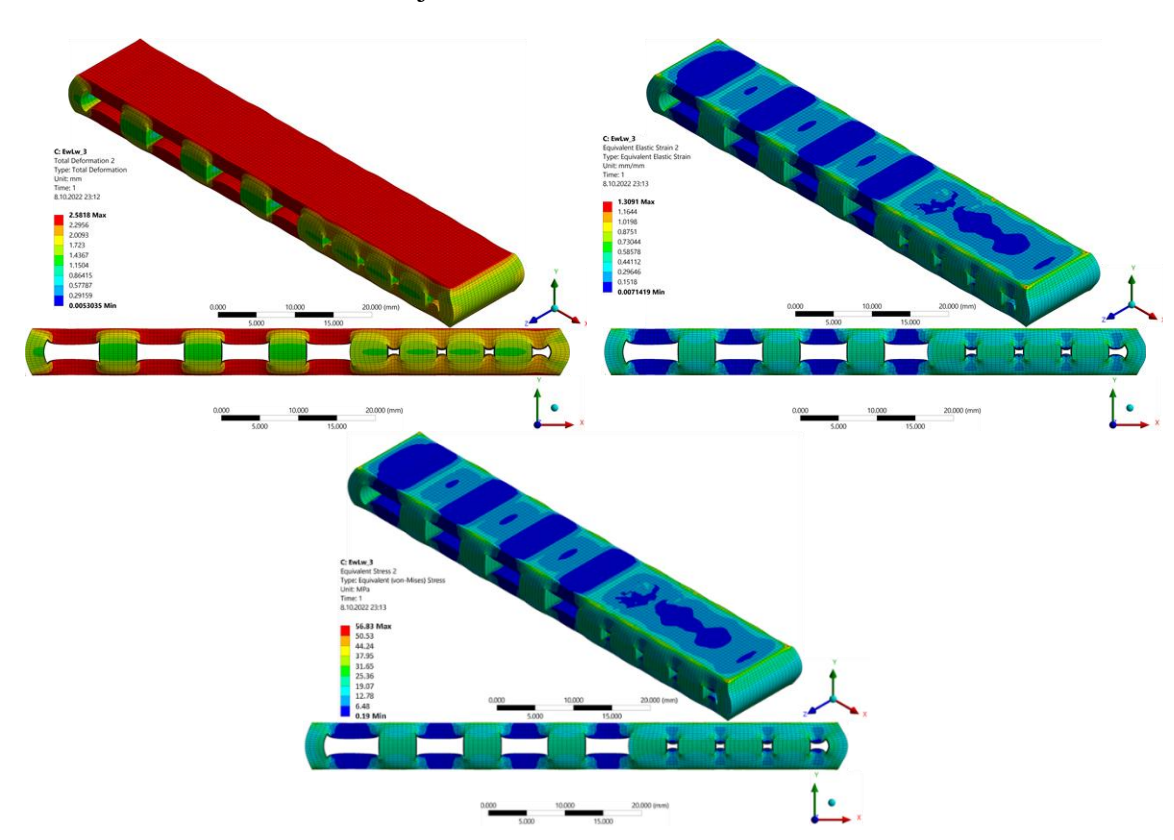


Fig. 8. Distributions of deformation, strain, and stress of wood cell wall Type C

Although Type D was basically Type A with three rows added on top of each other, it was seen that the deformation, stress, and strain values decreased gradually as the maximum went towards the middle row where the forces were applied. This effect can be seen in the contours (Fig. 9), where the deformation was higher in the right and left parts of the specimen, that is, in the edges, and relatively lower in the center. It is thought that the reason for this is that the barreling event took place at the edges and the column structures holding the middle part prevent it in this part. Moreover, while the wall was a

single layer at the edges, the fact that this wall had two layers at the cell junction points kept the structure strong relative to failure. The symmetry of the specimen was also effective relative to the homogeneity of stress and strain distributions.

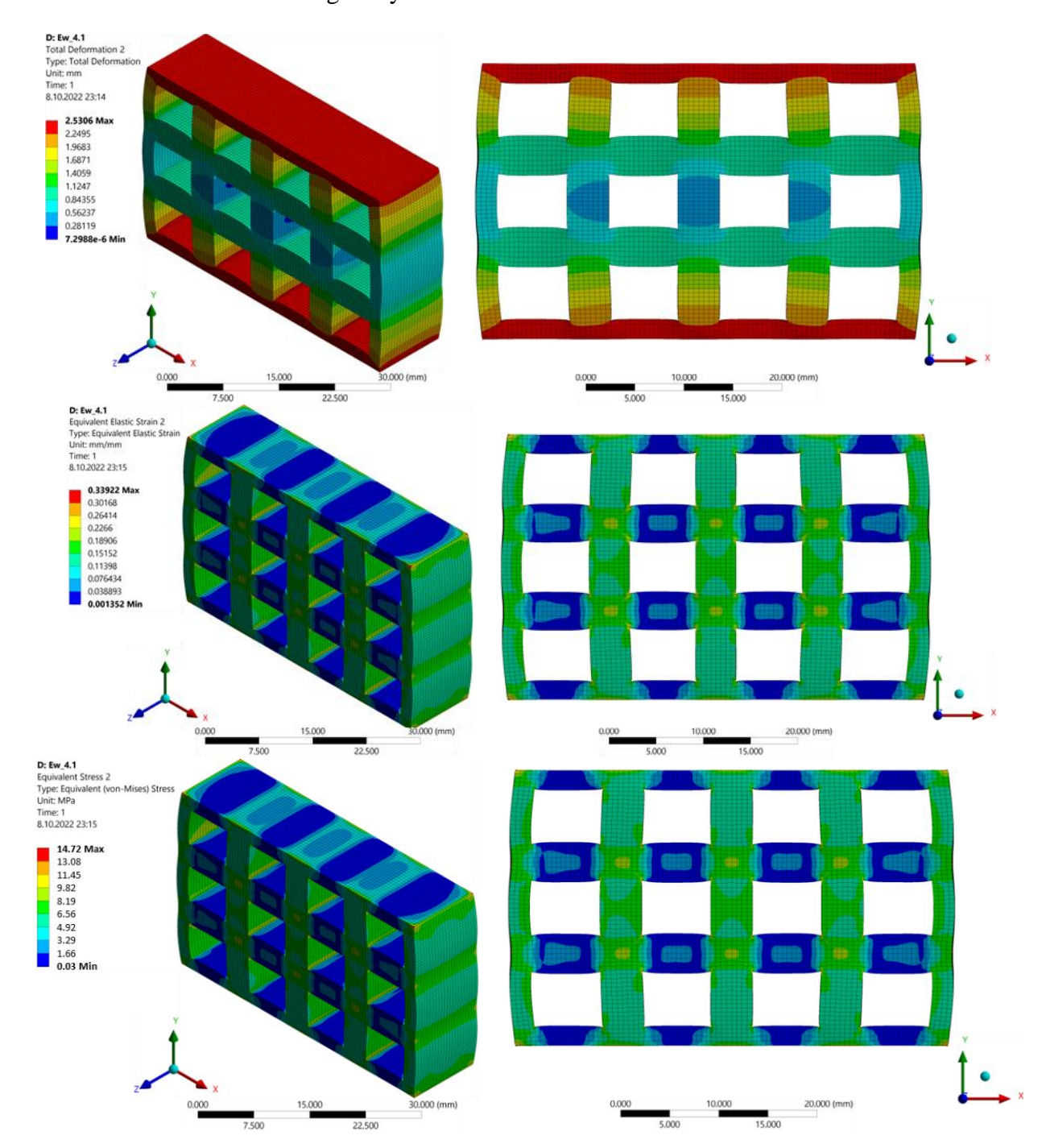


Fig. 9. Distributions of deformation, strain, and stress of wood cell wall Type D

Wood cell wall Type A, with 3 rows, middle row shifted (Type E), breaks the symmetry seen in the previous test samples, and when the deformation contour is examined, an increasing deformation rate can be seen from right to left (Fig. 10). The presence of a double wall on the rightmost vertical edge and the absence of a support

column in the middle at the far-left caused unbalanced stress distributions in the part. This is a harbinger that the stress and strain reach the maximum in the parts where the asymmetrical columns are connected, and that rupture may occur at these points in further compression.

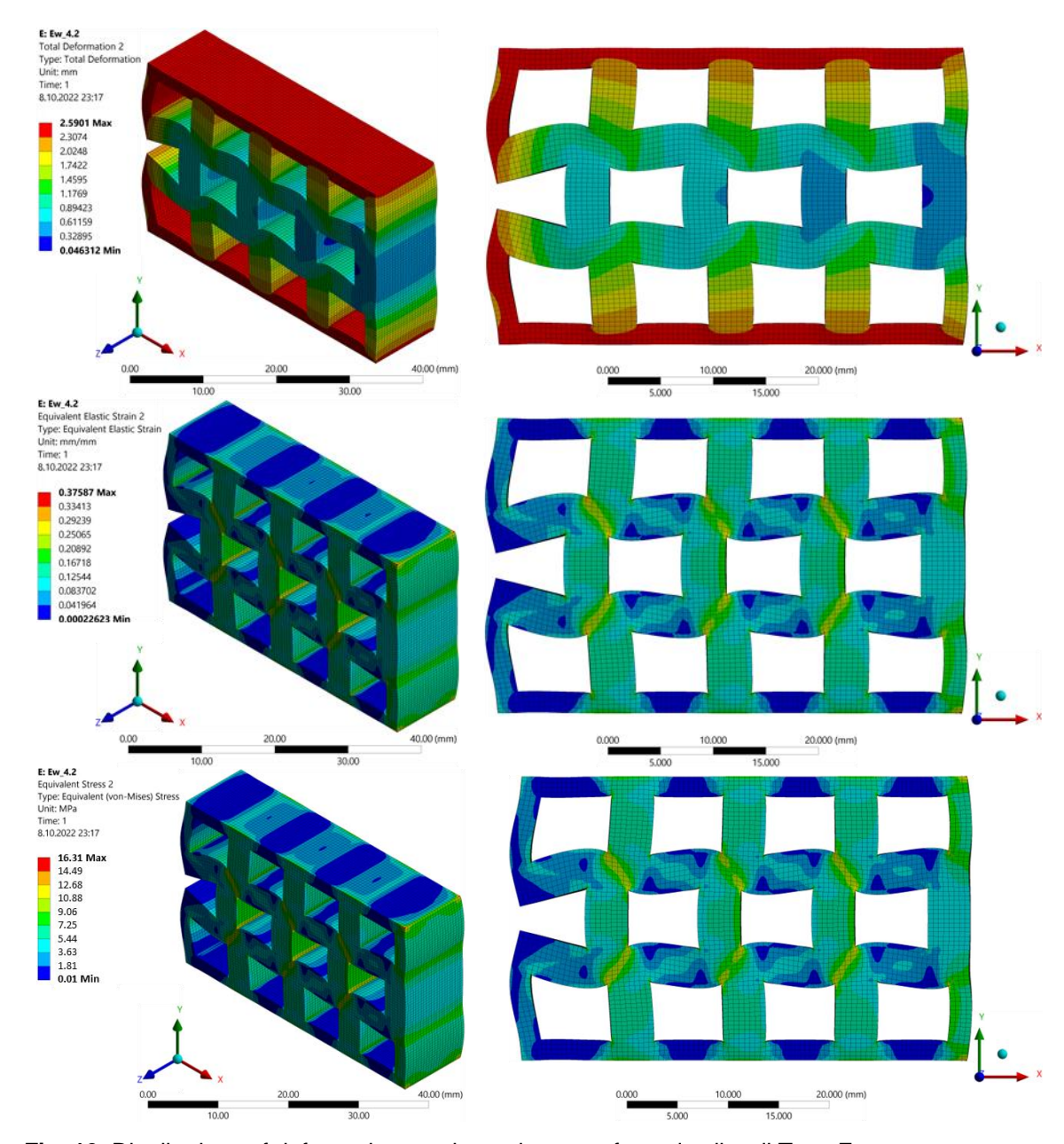


Fig. 10. Distributions of deformation, strain, and stress of wood cell wall Type E

Considering the contours shown in Fig. 11 occurring in Type F, the maximum stress generated was approximately 2.12 MPa lower than in Type E. The columns on both sides supporting the middle row were effective at this point. Angled potential rupture zones seen in Type E were replaced by vertical potential rupture zones.

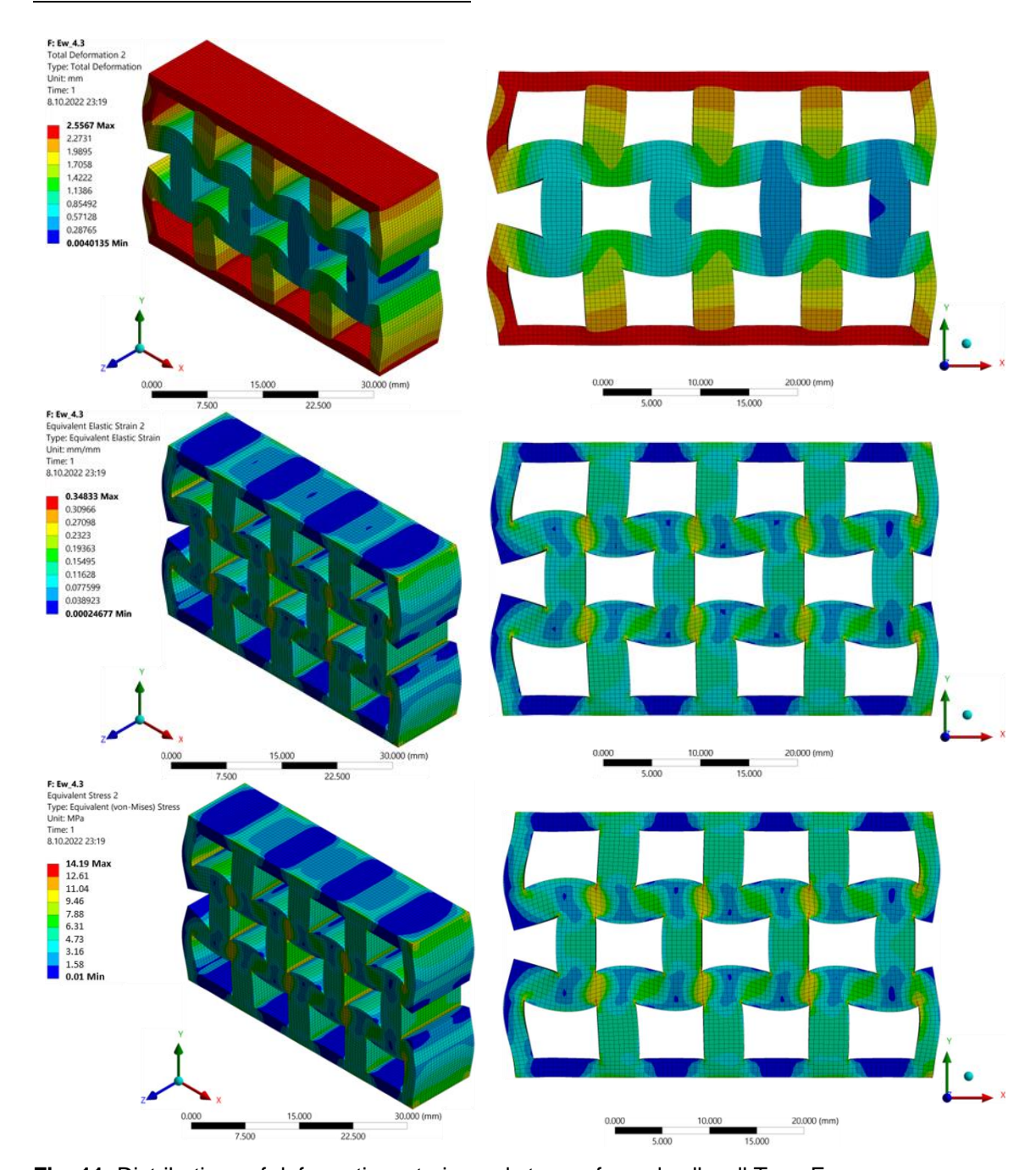


Fig. 11. Distributions of deformation, strain, and stress of wood cell wall Type F

To create realistic models for the numerical analysis, material properties and behavior under loads must be completely known (Chua *et al.* 2017). Furthermore, performing realistic numerical analysis can save time and avoid wastage of materials in the destructive testing. To achieve these goals, load and deformation behaviors of the AM models were figured out to determine the accuracy of the numerical analysis. Results demonstrated that FEM&A reasonably predicted the load-deformation behavior of the AM models with a maximum -45.9% difference in average stress.

It should be taken into consideration that anisotropic and orthotropic modeling of the structures requires detailed material properties such as full elastic constants. However, analysis by isotropic models is easier. In the literature, some studies evaluated the ABS parts produced by the FDM method. Recent studies have considered the influence of isotropy and anisotropy on the stress and tensile strength by FEM&A and destructive test (Bellini and Güçeri 2003), raster angle and air gap on mechanical properties (Górski *et al.* 2015), orientation (0°, 45°, and 90°) on tensile properties (Tang Dan *et al.* 2018), stretching, tensile strength, and hardness (Sikora *et al.* 2024), and internal support structures in different geometrical arrangements on compression test and FEM&A validation (Villalpando *et al.* 2014). In this respect, the AM gives opportunities for better figuring out the structural properties of wood and evaluating mechanical features over FEM&A (Wimmer *et al.* 2015).

CONCLUSIONS

- 1. As is well known, wood is a polar orthotropic material, but the additive manufacturing (AM) models did not replicate this structural property. Consequently, there were significant differences in the strength hierarchy, plateau regions, and other mechanical characteristics.
- 2. In this study, the samples were compressed in a tangential direction. To better understand the compression behavior of wood-inspired AM structures, samples also should be printed considering the fiber orientation of the wood and this will be done in a future study.
- 3. Numerical differences demonstrated that finite element analysis (FEA) is applicable to predict the compression behavior of AM with reasonable results. Not only the printing parameters, such as infill density, orientation, and layer height, and model design (geometry and size of the cells, *etc.*), but also the physical and mechanical properties of the filament used for layer accumulation defined the mechanical behavior of models.
- 4. White acrylonitrile butadiene styrene (ABS) filament was used to print the wood-based structures. Future research may explore the use of filaments modified with wood flour to produce real-like wood structures.

ACKNOWLEDGMENTS

The authors declare that they have no conflict of interest. Additionally, the research presented in the manuscript did not receive any external funding. The authors would like to thank the Department of Machinery and Metal Technologies and Civil Engineering.

REFERENCES CITED

ASTM D695 (2015). "Standard test method for compressive properties of rigid plastics," ASTM International, West Conshohocken, PA, USA.

Aydin, M., and Aydin, T. Y. (2022). "Bio-mimicry: Tree rings and three-dimensional printing – preliminary biomimetic experiments with fused deposition modeling using acrylonitrile butadiene styrene filament," *BioResources* 17(4), 6588-6597. DOI: 10.15376/biores.17.4.6588-6597

- Aydin, M. (2024). "Compression behavior of the wood-inspired cellular structure of acrylonitrile butadiene styrene," *Materialpruefung [Materials Testing]* 66(1), 66-74. DOI: 10.1515/MT-2023-0147/MACHINEREADABLECITATION/RIS
- Barbour, J. (2004). "Wood formation and properties | Wood Quality," in: *Encyclopedia of Forest Sciences*, Elsevier Ltd., Amsterdam, Netherlands, pp. 1840-1846. DOI: 10.1016/B0-12-145160-7/00039-9
- Bellini, A., and Güçeri, S. (2003). "Mechanical characterization of parts fabricated using fused deposition modeling," *Rapid Prototyping Journal* 9(4), 252-264. DOI: 10.1108/13552540310489631
- van Buijtenen, J. P. (2004). "Tree breeding, practices | Genetics and improvement of wood properties," in: *Encyclopedia of Forest Sciences*, Elsevier Ltd., Amsterdam, Netherlands, pp. 1466-1472. DOI: 10.1016/B0-12-145160-7/00082-X
- Buonamici, F., Volpe, Y., Furferi, R., Carfagni, M., Signorini, G., Goli, G., Governi, L., and Fioravanti, M. (2019). "Bamboo's bio-inspired material design through additive manufacturing technologies," in: *Digital Wood Design*, Springer Ltd., Amsterdam, Netherlands, pp. 809-826. DOI: 10.1007/978-3-030-03676-8_32/COVER
- Büyüksari Ü., As, N., and Dündar, T. (2017). "Mechanical properties of earlywood and latewood sections of scots pine wood," *BioResources* 12(2), 4004-4012. DOI: 10.15376/biores.12.2.4004-4012
- Cambaz, A., Gorgulu, Y. F., and Arat, H. (2022). "Analysing fluid-structure interaction with CFD and FEA on a marine double-wall LNG piping system," *Multidisciplinary Scientific Journal of Maritime Research* 36(1), 51-60. DOI: 10.31217/p.36.1.6
- Chen, C., Kuang, Y., Zhu, S., Burgert, I., Keplinger, T., Gong, A., Li, T., Berglund, L., Eichhorn, S. J., and Hu, L. (2020). "Structure–property–function relationships of natural and engineered wood," *Nature Reviews Materials* 5(9), 642-666. DOI: 10.1038/s41578-020-0195-z
- Chua, C. K., Wong, C. H., and Yeong, W. Y. (2017). Standards, Quality Control, and Measurement Sciences in 3D Printing and Additive Manufacturing, Elsevier Inc., Amsterdam, Netherlands.
- Chun-Won, K., Tsutsumi, J., and Jang, S.-S. (2001). "Mechanical behaviour of earlywood and latewood under longitudinal compression load," *Journal of the Korean Wood Science and Technology* 29(2), 76-83.
- Correa, D., Papadopoulou, A., Guberan, C., Jhaveri, N., Reichert, S., Menges, A., and Tibbits, S. (2015). "3D-printed wood: Programming hygroscopic material transformations," *3D Printing and Additive Manufacturing* 2(3), 106-116. DOI: 10.1089/3DP.2015.0022
- Das, A. K., Agar, D. A., Rudolfsson, M., and Larsson, S. H. (2021). "A review on wood powders in 3D printing: Processes, properties and potential applications," *Journal of Materials Research and Technology* 15, 241-255. DOI: 10.1016/J.JMRT.2021.07.110
- Eslami, H., Jayasinghe, L.B., and Waldmann, D. (2021). "Nonlinear three-dimensional anisotropic material model for failure analysis of timber," *Engineering Failure Analysis* 130, article 105764. DOI: 10.1016/j.engfailanal.2021.105764.
- Gebhardt, A. (2011). *Understanding Additive Manufacturing*, Carl Hanser Verlag, Munich, Germany. DOI: 10.3139/9783446431621
- Gibson, I., Rosen, D., Stucker, B., and Khorasani, M. (2021). *Additive Manufacturing Technologies*, Springer Nature Switzerland AG, Cham, Switzerland. DOI: 10.1007/978-3-030-56127-7

- Górski, F., Kuczko, W., Wichniarek, R., and Hamrol, A. (2015). "Computation of mechanical properties of parts manufactured by fused deposition modeling using finite element method," *Procedia CIRP* 36, 403-413. DOI: 10.1007/978-3-319-19719-7_35
- Hong, J. P., Barrett, J. D., and Lam, F. (2011). "Three-dimensional finite element analysis of the Japanese traditional post-and-beam connection," *Journal of Wood Science* 57, 119-125. DOI: 10.1007/s10086-010-1151-0
- ISO 604 (2002). "Plastics Determination of compressive properties," International Organization for Standardization, Geneva, Switzerland.
- Isoeai, A., Ishizu, A., and Nakano, J. (1989). "Residual lignin and hemicellulose in wood cellulose: analysis using new permethylation method," *Holzforschung* 43(5), 333-338. DOI: 10.1515/hfsg.1989.43.5.333
- Ibrahim, M., Badrishah, N. S., Sa'ude, N., and Ibrahim, M. H. I. (2014). "Sustainable natural bio composite for FDM feedstocks," *Applied Mechanics and Materials* 607, 65-69. DOI: 10.4028/WWW.SCIENTIFIC.NET/AMM.607.65
- Kam, D., Layani, M., Minerbi, B., Orbaum, D., Abrahami, S., Harush, B., Shoseyov, O., and Magdassi, S. (2019). "Additive manufacturing of 3D structures composed of wood materials," *Advanced Materials Technologies* 4(10), article ID 1900158. DOI: 10.1002/admt.201900158
- Kariz, M., Sernek, M., Obućina, M., and Kuzman, M. K. (2018). "Effect of wood content in FDM filament on properties of 3D printed parts," *Materials Today Communications* 14, 135-140. DOI: 10.1016/J.MTCOMM.2017.12.016
- Kollmann, F. F. P., Kuenzi, E. W., and Stamm, A. J. (1975). Principles of Wood Science and Technology, Springer, Berlin, Heidelberg, Berlin, Germany. DOI: 10.1007/978-3-642-87931-9
- Krapež Tomec, D., Balzano, A., Žigon, J., Šernek, M., and Kariž, M. (2022). "The effect of printing parameters and wood surface preparation on the adhesion of directly 3D-printed PLA on wood," *Journal of Renewable Materials* 10(7), 1787-1796. DOI: 10.32604/JRM.2022.019760
- Krapež Tomec, D., and Kariž, M. (2022). "Use of wood in additive manufacturing: Review and future prospects," *Polymers* 14(6), article 1174. DOI: 10.3390/polym14061174
- Li, W., Zhang, Z., Wang, X., Mei, C., Van Acker, J., and Van den Bulcke, J. (2021). "Understanding the effect of growth ring orientation on the compressive strength perpendicular to the grain of thermally treated wood," *Wood Science and Technology* 55(5), 1439-1456. DOI: 10.1007/S00226-021-01323-4/FIGURES/10
- Mai, J., Barata, E. D. O., Löschke, S. K., and Proust, G. (2022). "Fabricating wood-like textures on multicurved 3D printed architectural elements," *3D Printing and Additive Manufacturing* 9(2), 140-147. DOI: 10.1089/3DP.2021.0139
- Mańkowski, P., and Laskowska, A. (2021). "Compressive strength parallel to grain of earlywood and latewood of yellow pine," *Maderas. Ciencia y Tecnología* 23(1), 45-57. DOI: 10.4067/S0718-221X2021000100457
- Markstedt, K., Håkansson, K., Toriz, G., and Gatenholm, P. (2019). "Materials from trees assembled by 3D printing Wood tissue beyond nature limits," *Applied Materials Today* 15, 280-285. DOI: 10.1016/J.APMT.2019.02.005
- Montalvo Navarrete, J. I., Hidalgo-Salazar, M. A., Escobar Nuñez, E., and Rojas Arciniegas, A. J. (2017). "Thermal and mechanical behavior of biocomposites using

- additive manufacturing," *International Journal on Interactive Design and Manufacturing (IJIDeM)* 12(2), 449-458. DOI: 10.1007/S12008-017-0411-2
- Nicolau, A., Pop, M. A., and Coşereanu, C. (2022). "3D printing application in wood furniture components assembling," *Materials* 15(8), article 2907. DOI: 10.3390/MA15082907
- Öztürk, Y., and Burdurlu, E. (2024). "3D yazıcı ile yazdırılmış malzemede ahşap kaplama laminasyonunun eğilme direncine etkisi [Effect of wood veneer lamination on bending strength in 3D printd material]," *Journal of Bartın Faculty of Forestry* 26(1), 41-50. DOI: 10.24011/barofd.963190
- Saad, R. M. (2024). "The revolution of materials used in 3D printing applications in furniture & interior design," *Journal of Sustainable Design* 12(3), 67-74.
- Sikora, P., Gnatowski, A., and Gołębski, R. (2024). "Tests of mechanical properties of semicrystalline and amorphous polymeric materials produced by 3D printing," *MATEC Web of Conferences* 254, article 06003. DOI: 10.1051/matecconf/201925406003
- Tang Dan, B., Khodos, D. R., Khairallah, O., Ramlal, R., and Budhoo, Y. (2018). "The effect of the 3-D printing process on the mechanical properties of materials," *Conference Proceedings of the Society for Experimental Mechanics Series* 9, 91-99. DOI: 10.1007/978-3-319-62834-9_13/COVER
- Tao, Y., Wang, H., Li, Z., Li, P., and Shi, S. Q. (2017). "Development and application of wood flour-filled polylactic acid composite filament for 3D printing," *Materials* 10(4), article 339. DOI: 10.3390/MA10040339
- Tomec, D. K., Straže, A., Haider, A., and Kariž, M. (2021). "Hygromorphic response dynamics of 3D-printed wood-PLA composite bilayer actuators," *Polymers* 13(19), article 3209. DOI: 10.3390/POLYM13193209
- Tomec, D. K, and Kariž, M. (2022). "Use of wood in additive manufacturing: Review and future prospects," *Polymers* 14(6), article 1174. DOI: 10.3390/polym14061174
- Tomec, D. K, Balzano, A., Žigon, J., Šernek, M., and Kariž, M. (2022). "The effect of printing parameters and wood surface preparation on the adhesion of directly 3D-printed PLA on wood," *Journal of Renewable Materials* 10(7), 1787-1796. DOI: 10.32604/JRM.2022.019760
- Toumpanaki, E., Shah, D. U., and Eichhorn, S. J. (2021). "Beyond what meets the eye: Imaging and imagining wood mechanical–structural properties," *Advanced Materials* 33(28), article ID 2001613. DOI: 10.1002/adma.202001613
- Ueda, K. (2024). "Interlocking 3D-printed bars, trusses and space frames to build arbitrarily large structures," *Journal of Additive Manufacturing Technologies* 14(3), 239-250. DOI: 10.1007/s12008-024-0657-4
- Villalpando, L., Eiliat, H., and Urbanic, R. J. (2014). "An optimization approach for components built by fused deposition modeling with parametric internal structures," *Procedia CIRP* 17, 800-805. DOI: 10.1016/j.procir.2014.02.050
- Wang, J., Yang, K., Li, W., Wang, X., Van den Bulcke, J., and Van Acker, J. (2023). "The impact of earlywood and latewood on the compressive stress of thermally modified Douglas fir," *Forests* 14(7), article 1376. DOI: 10.3390/f14071376
- Wimmer, R., Steyrer, B., Woess, J., and Mundigler, N. (2015). "3D printing and wood," Journal of Wood Science and Technology 11(1), 201-210. DOI: 10.1007/s12008-015-0657-4

- Yan, S., Eichhorn, S. J., and Toumpanaki, E. (2022). "Numerical simulation of transverse compression and densification of wood," *Wood Science and Technology* 56(4), 1007-1027. DOI: 10.1007/s00226-022-01388-9
- Yilmaz Aydin, T. (2022). "Do it yourself furniture: Part A Designing fittings for an easy to manufacture hybrid chair," *Mobilya ve Ahşap Malzeme Araştırmaları Dergisi* 5(1), 50-60. DOI: 10.33725/MAMAD.1129596
- Yilmaz, A. T., and Aydin, M. (2017). "Three dimensional finite element analysis of compression behavior of oriental beech," *Düzce Üniversitesi İleri Teknoloji Bilimleri* 6(3), 795-803.
- Zhang, J. S., Yang, Y. T., Qin, Z. K., Luo, J. J., Gao, W., and Wei, S. L. (2016).
 "Research progress of the modified wood powder for 3D printing," in: *Proceedings of the 2016 4th International Conference on Mechanical Materials and Manufacturing Engineering*, Vol. 79, S. H. Zhu, (ed.), Atlantis Press, Amsterdam, Netherlands, pp. 574-577. DOI: 10.2991/MMME-16.2016.217

Article submitted: May 3, 2024; Peer review completed: June 15, 2024; Revised version received: June 28, 2024; Accepted: August 12, 2024; Published: August 26, 2024. DOI: 10.15376/biores.19.4.7493-7512